

****TITLE****

*ASP Conference Series, Vol. **VOLUME**, **YEAR OF PUBLICATION***

****NAMES OF EDITORS****

The Unidentified InfraRed Features after ISO

E. Peeters, L.J. Allamandola, D.M. Hudgins

*NASA-Ames Research Center, Space Science Division, MS: 245-6,
Moffett Field CA 94035-1000, U.S.A.*

S. Hony

*RSSD-ESA/ESTEC, PO Box 299, 2200 AG Noordwijk, The
Netherlands*

A.G.G.M. Tielens

*Kapteyn Institute & SRON National Institute for Space Research, P.O.
Box 800, 9700 AV Groningen, The Netherlands*

Abstract. The Infrared Space Observatory (ISO) has provided the first complete mid-IR spectra for a wide range of objects. Almost all of these spectra are dominated by the well-known infrared emission features at 3.3, 6.2, 7.7, and 11.2 μm , the so-called Unidentified Infra-Red (UIR) features. Besides the major features, there is an array of minor features and broad plateaux stretching from 3 to 20 μm which reveal subtle details of conditions in the emission zones and properties of the carriers. Generally attributed to the vibrational relaxation of UV-pumped Polycyclic Aromatic Hydrocarbon molecules (PAHs) containing some 50–100 C-atoms, these UIR spectra are a treasure trove of information.

The ISO spectra have, for the first time, allowed a systematic analysis of the spectral characteristics of the UIR features in a wide variety of environments. The peak positions, profiles, and relative strengths of the major features vary from source to source and spatially within sources. Variations in the 6.2 and 7.7 μm features are particularly noteworthy; the former peaks between 6.25–6.3 μm in many PNe, but falls at 6.2 μm in RNe and H II regions. Similarly, the broad 7.7 μm feature consists of major components at 7.6 and “7.8” μm whose relative strengths vary. The 7.6 μm component dominates in H II regions and reflection nebulae, while the “7.8” μm feature takes over in most PNe. These specific profiles are not unique to certain object types but can occur within each individual source. While the 3.3 and 11.2 μm also show variations in peak position and profile, these are much less pronounced. In addition, the 3.3 μm feature intensity correlates quite well with that of the 11.2 μm feature, a correlation which does not extend to the CH modes between 12 and 14 μm . Also, variations occurs in the relative strengths of the CC modes in the 6–9 μm range relative to the CH modes 3.3 and 11.2 μm . Such behavior requires that the UIR features are carried by a family of related compounds whose detailed physical and/or chemical characteristics vary

in response to local physical conditions. Here, we review ISO and recent ground-based observations and assess some of their implications.

1. Introduction

The infrared spectra of a wide variety of objects associated with dust and gas – including H II regions, post-AGB stars, PNe, young stellar objects (YSOs), the diffuse ISM and galaxies – are dominated by emission features at 3.3, 6.2, 7.7, 8.6, 11.2 and 12.7 μm , (cf. Gillett et al., 1973; Geballe et al., 1985; Cohen et al., 1986; Cox & Kessler, 1999). Often, these features are accompanied by broad underlying emission plateaux. Since the carriers of these features remained a mystery for almost a decade, the initial name for these features, the Unidentified InfraRed (UIR) emission features, is still in use. However, there is also an unfortunate proliferation of other names (Table 1). Here we use the term UIRs to refer to these features.

In the early '80s, it was recognized that the UIR features coincide with the vibrational modes characteristic of aromatic materials (Duley & Williams, 1981). Since then, many different carriers have been proposed such as Hydrogenated Amorphous Carbon (HAC, e.g. Duley & Williams, 1983; Borghesi et al., 1987), Quenched Carbon Composites (QCC, e.g. Sakata et al., 1984), Polycyclic Aromatic Hydrocarbons (PAHs, e.g. Allamandola et al., 1989; Puget & Léger, 1989), Coal (e.g. Papoular et al., 1989), nanodiamonds (Jones & d'Hendecourt, 2000), Rydberg matter (Holmlid, 2000) and most recently Locally Aromatic Polycyclic Hydrocarbons (Petrie et al., 2003).

While the vibrational spectrum of (almost) any exclusively aromatic material can provide a global fit to the observed UIR features, they are generally attributed to *small* aromatic hydrocarbon species. The main argument for this is the detection of the UIR features in reflection nebulae far from illuminating stars and the independence of the color temperature with the distance from the star. Taken together, these observations indicate that the carriers of the UIR features can be excited to very high “temperatures” in such cold environments upon absorption of a *single* FUV photon (Sellgren, 1984). This requires the emitting species to be very small, containing a finite number of oscillators. Classical 0.1 μm size grains are too large and do not become hot enough to emit at mid-infrared wavelengths in these environments. Hence the UIR features are attributed to species of the order of 10 Å (Sellgren, 1984). This corresponds to molecules containing ~ 50 –100 carbon atoms (e.g. Tielens, 1993; Tielens et al., 1999). This aspect of the UIR feature phenomenon has now been reinforced by ISO and IRTS observations which reveal that the mid-infrared spectra of the (diffuse) ISM is dominated by these IR emission features (see Onaka, these proceedings; Mattila et al., 1996; Onaka et al., 1996; Boulanger et al., 1998a; Boulanger, 1999; Boulanger et al., 2000; Onaka, 2000). It should be emphasized that, at the smallest scales, all of the proposed grain carriers (HAC, QCC, coal, ...) share an aromatic hydrocarbon structure with PAH molecules. However, some of these carriers may vary in detail from PAH molecules (adopting their chemical definition), even at sizes required by the energetics, by including aliphatic hydrocarbon chains, by containing substitution of other elements such

Table 1. Possible names for the IR emission band family found in the literature to date.

UIRs	Un-identified InfraRed emission features
IEFs / IEBs	Infrared Emission Features/Bands
AEFs / AFE	Aromatic Emission Features / Aromatic Feature Emission
AIBs	Aromatic Infrared (emission) Bands
PAHs	Polycyclic Aromatic Hydrocarbon bands/features
OIRs	Over-identified InfraRed emission features

as N or O for a C atom in a PAH, or by having D or molecular sidegroups substituting for an H atom in a PAH. However, limits on the presence of other functional groups are very strict (Tielens et al., 1999). Methyl groups ($-\text{CH}_3$) are the most abundant at 0.02 of aromatic H (or equivalently ~ 0.01 relative to aromatic C). Other substitutions such as OH and NH_2 are less abundant than 0.01 relative to aromatic H. There is some spectroscopic evidence for the presence of oxygen bonded in the form of carbonyl groups ($-\text{C}=\text{O}$; much less than 0.01 relative to aromatic C). All other species are at a very low level.

In short, the excitation of such small species should be discussed in molecular physics terms. An absorption of a FUV photon by a small aromatic hydrocarbon induces a transition to an upper electronic state. The excited molecule then makes rapid isoenergetic transitions to highly vibrationally excited levels of the ground electronic state. Subsequently, this highly vibrationally excited molecule relaxes, mainly by IR emission in the CC and CH fundamental vibrational modes (Allamandola et al., 1989, see Li, these proceedings). In this way, small aromatic hydrocarbons leave their signature in the form of the UIR features.

Mid-infrared spectra from many objects are dominated by the UIR emission features. Remarkably 20-30% of the Galactic IR radiation is emitted in these UIR features and 10-15% of the cosmic carbon is locked up in the UIR carriers (Snow & Witt, 1995).

Being so widespread and abundant, they play a crucial role in several astrophysical processes. Aromatic units are the building blocks in the cosmic carbon condensation route (Frenklach & Feigelson, 1989; Tielens, 1990, 1997; Tielens & Charnley, 1997; Cherchneff et al., 2000). The UIR carriers dominate the heating and cooling of the ambient interstellar medium (ISM) via photoelectric ejection (Verstraete et al., 1990; Bakes & Tielens, 1994), infrared emission and gas-grain collisional cooling (Aannestad & Kenyon, 1979; Dwek, 1986). In addition, they influence the charge balance and in this way – through their influence on the equilibrium state of chemical reactions – gas-phase abundances in interstellar (IS) clouds (Lepp & Dalgarno, 1988; Bakes & Tielens, 1998). In particular, they might reduce the gas-phase D/H ratio (Draine, 2003; Peeters et al., 2004a). Due to their large surface areas, they also affect the on-going surface chemistry and so play a significant role in IS chemistry (Tielens & Allamandola,

1987). Lastly, they are an important, chemically accessible, source of prebiotic organic material.

Although the presence of aromatic hydrocarbon species in space is now generally accepted, today, specifics of the emitting population remain elusive. Progress is being made however (e.g. Hudgins & Allamandola, these proceedings) and strong constraints are placed on molecular structures (Allain *et al.*, 1996; Hony *et al.*, 2001), sizes (Schutte *et al.*, 1993), heteroatom substitution (Peeters *et al.*, 2002; Bauschlicher *et al.*, 2004), charge balance (Allamandola *et al.*, 1999; Wagner *et al.*, 2000; Le Page *et al.*, 2003) and related properties (Robinson *et al.*, 1997; Cr  t   *et al.*, 1999; Chan *et al.*, 2001). The combination of the astronomical observations with the laboratory and theoretical studies increases our understanding of how the local environment and/or the history influence the composition of this population; and vice-versa, how the aromatic hydrocarbon molecules influence the local physical and chemical processes. Such insight is also essential if we want to use the UIR emission features as tools for probing the universe.

Many studies have attempted to solve pieces of this puzzle and here we review the progress made in the observational domain since the launch of the Infrared Space Observatory (ISO). With its complete access to the 2.3–197 μm , wavelength range, ISO allowed the study of the UIR features in all their glory. Complemented with observations by the IRTS and recent ground-based instruments, these ISO observations have opened the doorway to the exploitation of the UIR features as probes of a wide variety of astronomical environments – from RNe to galaxies.

In the following, Sect. 2 highlights the omnipresent and rich UIR spectrum. Its spectral variations and their implications are extensively discussed in Sects. 3 and 4. The UIR emission features as diagnostic tools are considered in Sect. 5. Finally, Sect. 6 gives a summary and looks to the future.

2. The UIR spectrum

Fig. 1 illustrates the spectral richness and some of the variations of the UIR spectra. Clearly, many weaker features are present apart from the major UIR features at 3.3, 6.2, 7.7, 8.6, 11.2 and 12.7 μm . Some of these features are perched on top of emission plateaux of variable strength. These plateaux are treated in 2 ways. Either they are assumed to be part of the individual features and fitted with Lorentzians in combination with a power-law continuum (Fig. 6, e.g. Boulanger *et al.*, 1998b; Verstraete *et al.*, 2001). Or, they are considered independently of the individual features and then local spline continua are used (Fig. 1, e.g. Hony *et al.*, 2001; Peeters *et al.*, 2002). The latter is based upon early observations revealing a different spatial distribution for the plateaux and the features (Bregman *et al.*, 1989). Adopting the latter method, the 3.3 μm feature is situated on a broad plateau and is often accompanied by features at 3.4 and/or 3.5 μm . Two weaker features are found at 5.2 and 5.7 μm . The 6.2 and 11.2 μm features are accompanied with satellite features at 6.0, 11.0 and sometimes at ~ 6.6 μm . The broad 7.7 μm complex is composed of at least 2 subcomponents at 7.6 and 7.8 μm . Some sources exhibit more substructures e.g. near 7.2 to 7.4 and 8.2 μm (Moutou *et al.*, 1999a,b; Peeters *et al.*, 2002). A broad emission plateau of variable strength is present underneath the 6.2, 7.7 and

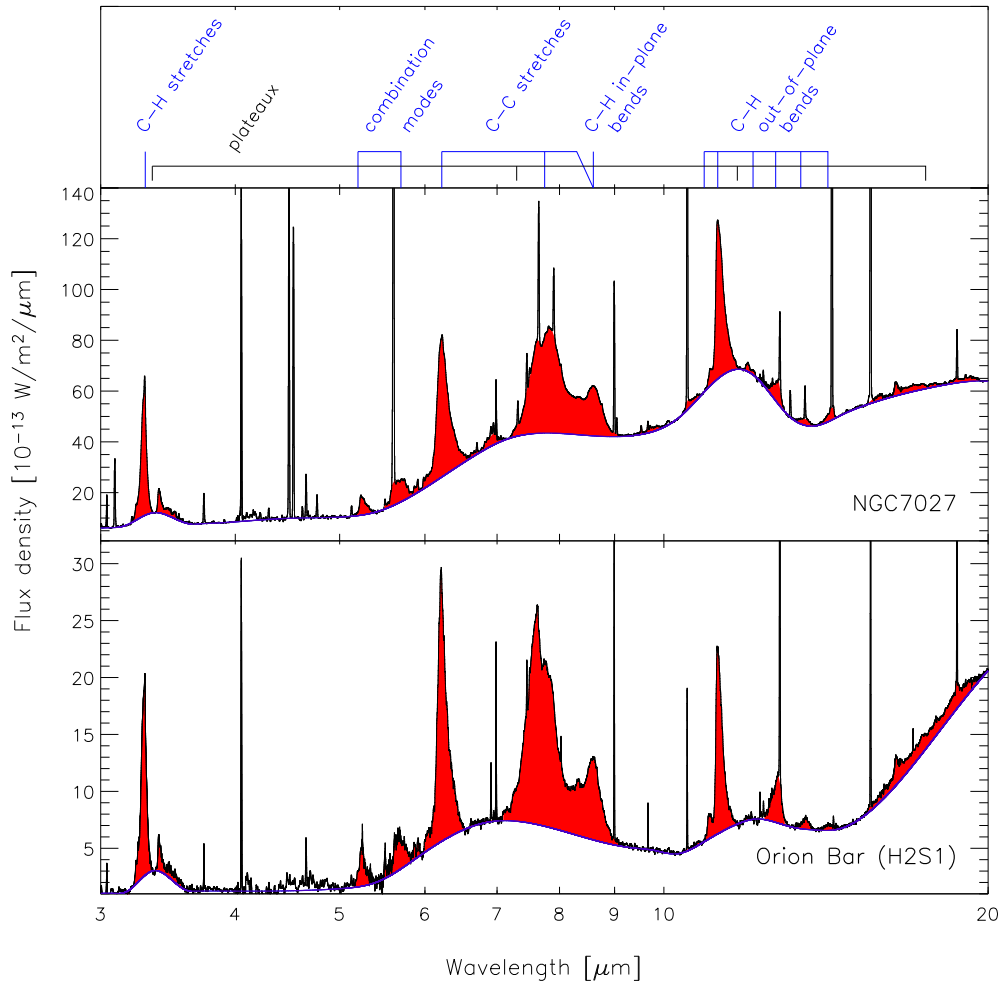


Figure 1. The ISO-SWS spectra of the planetary nebula NGC 7027 and the Photo-Dissociation region at the Orion Bar illustrate the richness and variety of the UIR spectrum. Also indicated are the aromatic mode identifications of the major UIR features.

8.6 μm features. The onset of this emission plateau seems to be variable and falls longwards of $\sim 6 \mu\text{m}$ while it extends to $\sim 9 \mu\text{m}$. The out-of-plane CH bending modes are present at 10.8, 11.0, 11.2, 12.0, 12.7, 13.2 and 14.5 μm and also sit on a broad emission plateau. At even longer wavelengths, a new feature has been reported at 16.4 μm (Moutou et al., 2000; Van Kerckhoven et al., 2000) as well as a weak emission plateau between 15 and 20 μm (Van Kerckhoven et al., 2000). It should be emphasized that not all sources show all these emission features at the same time and their peak position and relative strength vary as discussed below.

The importance of this family of emission features cannot be over emphasized. These emission features are now found in almost all environments includ-

ing diffuse ISM, the edges of molecular clouds, reflection nebulae, young stellar objects, H II regions, star forming regions, some C-rich WR stars, post-AGB stars, planetary nebulae, novae, normal galaxies, starburst galaxies, most Ultra-Luminous IR galaxies (ULIRGs) and AGNs. Thus, it is no exaggeration to say that the niche for the UIR carriers is the universe.

3. Feature Positions and Profiles

Until quite recently, most of the interstellar emission features were considered to be more-or-less invariant in position and profile. The $3.3\ \mu\text{m}$ feature is the exception. High resolution observations by Tokunaga et al. (1991) and Kerr et al. (1999) showed slight variations in peak position and profile. Although some minor variations were noted, by and large the $6.2\ \mu\text{m}$ feature was considered fixed at $6.2\ \mu\text{m}$, regardless of the reported shift in peak position by Molster et al. (1996). The " 7.7 " μm feature was generally treated similarly in spite of earlier papers showing this feature is comprised of at least two variable components (e.g. Bregman, 1989; Cohen et al., 1989). It has long been recognized that the $7.7\ \mu\text{m}$ complex appears either with a dominant $7.6\ \mu\text{m}$ component or with the dominant component peaking at $7.8\text{--}8\ \mu\text{m}$ (Bregman, 1989; Cohen et al., 1989; Molster et al., 1996; Roelfsema et al., 1996; Moutou et al., 1999a,c; Peeters et al., 1999). The former profile is associated with H II regions and the latter with planetary nebulae (Bregman, 1989; Cohen et al., 1989).

3.1. Source to source variations

Using ISO-SWS spectra, Peeters et al. (2002) and van Diedenhoven et al. (2004) have carried out a detailed study of the well-known UIR features in a large sample of reflection nebulae, H II regions, YSOs, evolved stars and galaxies. These authors found that the peak position of the UIR features clearly varies from source to source (see Fig. 2). In addition, distinct differences are found in their profiles. In particular, the $6.2\ \mu\text{m}$ profile is very asymmetric with a steep blue wing and a red tail when peaking at the shortest wavelengths ($6.22\ \mu\text{m}$) but it is generally far more symmetric when peaking at the longest wavelengths (i.e. $6.3\ \mu\text{m}$). Nevertheless, more asymmetric profiles peaking at $6.3\text{--}6.4\ \mu\text{m}$ are also reported for hydrogen deficient environments (Harrington et al., 1998; Chiar et al., 2002). The $7.7\ \mu\text{m}$ complex is indeed comprised of two components, one at $7.6\ \mu\text{m}$ and one at " 7.8 " μm . The feature varies from a profile with a dominant to a minor $7.6\ \mu\text{m}$ component while simultaneously shifting, as a whole, to longer wavelengths. The peak position of the " 7.8 " component is highly variable and ranges from 7.8 up to $8\ \mu\text{m}$. Several sources show an additional subcomponent between 7.2 and $7.4\ \mu\text{m}$ (see also Moutou et al., 1999a,b). The profile of the $8.6\ \mu\text{m}$ feature is clearly symmetric and similar for all sources. However, distinct shifts in peak position are also observed for this feature. Four sources are known to date that show a peculiar $8.6\ \mu\text{m}$ feature (see also Roelfsema et al., 1996; Verstraete et al., 1996; Peeters et al., 2004c). A very limited number of sources does not show a $7.7\ \mu\text{m}$ complex nor a $8.6\ \mu\text{m}$ feature but instead exhibit a broad emission feature peaking at $8.22\ \mu\text{m}$. This is clearly distinct from the $8\ \mu\text{m}$ emission feature found in some post-AGB stars. The $3.3\ \mu\text{m}$ profile is clearly symmetric when positioned at the shortest wavelengths and asymmetric

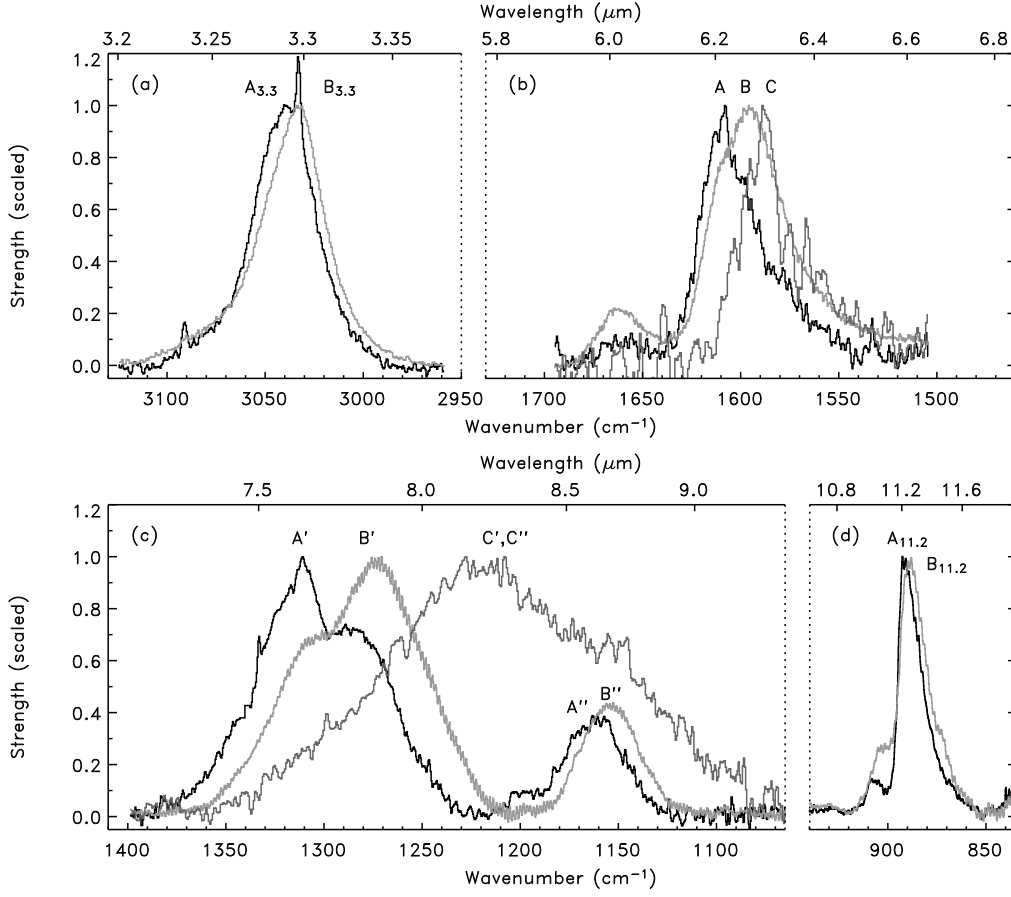


Figure 2. An overview of the source to source variations in the position and profile of the 3–12 μm UIR features. For all features, class *A* peaks at the shortest wavelengths (black line), and class *B* peaks at longer wavelength. In the 6–9 μm region, another class (*C*) is defined peaking at even longer wavelength with a unique spectral appearance. For details see Peeters et al. (2002) and van Diedenhoven et al. (2004).

when peaking at slightly longer wavelengths. The former profile has a similar peak position and FWHM as the Type 1 profile of Tokunaga et al. (1991), the latter has a peak position similar to their Type 2 but is much wider. The 11.2 μm profile comprises a steep blue rise and a red tail and only shows small variations in both peak position and profile.

The observed pronounced contrast in the spectral variations for the CH modes versus the CC modes is striking : the peak wavelengths of the features attributed to CC modes (6–9 μm) vary by $\sim 25\text{--}50\text{ cm}^{-1}$, while for the CH modes (3.3 and 11.2 μm features) the variations are smaller, $\sim 4\text{--}6.5\text{ cm}^{-1}$. Moreover, these profile variations in the CC modes are directly linked with each other, i.e. the 6.2 μm profile *A* is correlated with the 7.7 μm profile *A'* and the 8.6 μm profile *A''* while the 6.2 μm profile *B* is correlated with the 7.7 μm profile *B'* and

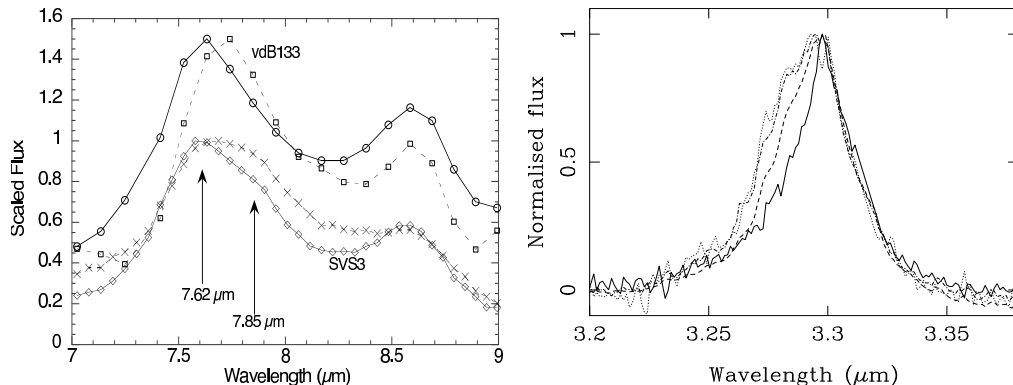


Figure 3. **(left)** The 7.7 and 8.6 μm UIR features are shown for two positions within the reflection nebulae vdB133 (top two traces) and SVS3 (lower two traces) obtained with ISOCAM-CVF. Courtesy of Bregman & Temi (2003, 2004). **(right)** The observed variations of the 3.3 μm feature in the Red Rectangle with angular distance from the central star. The spectra shown are the result of continuum subtraction followed by normalization to a common peak intensity. Solid line - on-star spectrum; dashed line - 2.6'' spectrum; dot-dash line - 3.8''; dotted line - 5'' spectrum. The growth of a shoulder with increasing distance from the star is evident. Courtesy of Song et al. (2003a,b).

the 8.6 μm profile B''. In contrast, the CH feature profile variations appear less connected to each other or to those found for the CC modes.

As already noted by Bregman (1989) and Cohen et al. (1989) for the 7.7 μm complex, the specific profile of the CC modes (but less for the CH modes) depend directly on the type of object. All H II regions, non-isolated YSOs and reflection nebulae exhibit class A emission features (black line in Fig. 2). Lines-of-sight towards the (diffuse) ISM also belong to this group (see Onaka, these proceedings, Mattila et al., 1996; Moutou et al., 1999c; Uchida et al., 2000; Kahanpää et al., 2003). In contrast, those of most planetary nebulae and isolated Herbig AeBe stars are highly variable and are all shifted towards longer wavelengths (exemplified in Fig. 2 by class B). Important exceptions to such classification are the post-AGB stars who emit features from all classes A, B and C. Furthermore, it should be emphasized that while class A and C show little to no variation in their profiles, large difference are present within class B.

3.2. Variations within a source

The studies outlined above have concentrated on the variations between the *entire* integrated UIR spectra from various types of sources. These studies reveal interesting variations with source type. It is important to investigate these variations on a smaller spatial scale as they hold the promise of probing some of the physical parameters that influence the emergent UIR spectrum.

UIR feature variations within a source were first reported for the 3.3 μm feature in the Red Rectangle (Kerr et al., 1999). Approaching the star, the 3.3 μm profile shifts from a Type 1 profile to a Type 2 profile (Fig. 3, left panel

Kerr et al., 1999; Song et al., 2003a,b). Hence close to the star, the $3.3\ \mu\text{m}$ feature has the same peak position but a smaller width than class B while further from the star, they are similar to those of class A which is associated with H II regions and the ISM. The $3.3\ \mu\text{m}$ profile in the ISO-SWS spectrum (integrated over a $14'' \times 20''$ beam) belongs to class B and hence has a similar peak position as Type 2 features but with a larger FWHM. The latter is likely caused by the increasing blue shoulder (as seen in the spatial study), however, it is unclear why the peak position is not influenced by this.

Similarly, the 7.7 and $8.6\ \mu\text{m}$ UIR features in the Red Rectangle show significant spatial variations (Song et al., 2003b, Song et al. in preparation). In particular, the $7.7\ \mu\text{m}$ complex evolves from a feature with a minor to one with a dominant $7.6\ \mu\text{m}$ component with larger distance from the star. Consistent with this, the $8.6\ \mu\text{m}$ UIR feature shifts to shorter wavelengths with distance from the star. Hence, with increasing distance from the star, these features seem to evolve from those observed in the ISO-SWS (integrated) spectra of PNe and the Red Rectangle to those of H II regions and the ISM. In addition, the variations of the 7.7 and $8.6\ \mu\text{m}$ features within the Red Rectangle show the same correlated behavior as found from source to source.

Bregman & Temi (2003, 2004) have studied the spatial behavior of the UIR features in three RNe using ISOCAM-CVF observations. ISOCAM allows a spatial resolution of 1.5 , 3 , 6 or $12''$ whereas ISO-SWS spectra integrate a larger area ($14'' \times 20''$). Thus, although ISO-SWS spectra of RNe show similar UIR emission features, these authors found clear variations in the $7.7\ \mu\text{m}$ UIR feature (see Fig. 3, right panel). In particular, within vdB133, the profile shifts from class A' to class B' in crossing the nebula but in SVS3 both components are present with variable strength. The latter profile is very similar to those in Planetary Nebulae with a dominating “ 7.8 ” μm peaking at the shortest wavelengths and is found in regions closer to the illuminating star.

3.3. Implications

These observations suggest that in all sources variations in the profile and peak position occur on a small spatial scale. In addition, - in contrast to what analysis of the integrated spectra of sources might suggest - the specific profiles are not unique to certain object types. In particular, it should be noted that the profiles positioned at longest wavelengths (class B and Type 2) are found close to the illuminating star for the three sources (2 RNe and 1 post-AGB star) discussed above. With increasing distance from the illuminating star, the UIR feature profiles are more like those found in the integrated spectra of H II regions and the ISM. Thus, while the average (or predominant) profile present within a source does depend on object type, the variations within sources demonstrate that this likely reflects the reaction of the PAH family to the very local physical conditions rather than a difference in chemical history. Thus, the profile variations between source types reflect the systematic variations in physical conditions with source type.

The observed variations in the peak position and profile of the various UIR features provide direct clues to the characteristics of their carriers and their reaction to a changing environment. Several different properties/characteristics are proposed to explain them. Amongst these are anharmonicity, different subcom-

ponents with variable strength, substituted/complexed PAHs, isotope variations, clustering, ... (Verstraete et al., 1996; Pech et al., 2002; Verstraete et al., 2001; Peeters et al., 2002; Wada et al., 2003; Song et al., 2003a; Bregman & Temi, 2004; van Dienenhoven et al., 2004, Hudgins & Allamandola, these proceedings). Here we will focus on two observational facts and their implications within the framework of the PAH model – the (asymmetric) profiles and the 6.2 μm UIR feature.

The (asymmetric) profiles Barker et al. (1987) has proposed a model to explain the observed (red shaded) profiles of the 3.3, 6.2, and 11.3 μm UIR features. In this interpretation, the red shading comes from the emission from highly vibrationally excited PAHs. In this case, emission from levels above the first excited state become important. Due to the anharmonic nature of the potential well, these feature spacings become smaller the higher up the vibrational ladder one samples and emission between these levels falls progressively to the red producing a red wing reminiscent of the observed wing. In addition, anharmonic coupling of the emitting mode with other modes also shifts the peak position of the emitting feature to lower energies. Integrating over the energy cascade as the emitting species cools down will then, in a natural way, give rise to a red shaded profile. Recently, Pech et al. (2002) and Verstraete et al. (2001) have modeled the IR emission spectrum of PAHs based upon extensive laboratory studies of the shift in peak position as a function of temperature of the emitter which is a direct measure of the anharmonicity (Joblin et al., 1995). They obtained excellent fits to the observed profiles of the 3.3, 6.2 and 11.2 μm features.

The UIR feature profiles in integrated spectra of many sources are very similar, irrespective of the illuminating radiation field. As exemplified by the model study of Verstraete et al. (2001), this indicates that the typical size of the emitting PAH is larger in regions which are illuminated by hotter stars. This coupling between size and the "color" of the illuminating radiation field may be a natural consequence of emission from a smooth size distribution of PAH species; that is, the smallest PAHs which can survive in a radiation field will depend on the average photon energy in the illuminating FUV field (Allamandola et al., 1989).

The variation in the peak position of the 6.2 μm UIR feature Laboratory and theoretical studies show that PAH cations have strong CC modes longwards of 6.3 μm with the largest PAH cations emitting near 6.3 μm . This behavior is consistent with the limit of graphite which shows an emission mode at 6.3 μm (Draine, 1984). As a consequence, such species cannot explain a peak position as short as 6.2 μm . Possibly, this shift in the peak position of the 6.2 μm UIR feature results from the substitution of N into the internal PAH rings in the ISM, although the chemical processing involved is presently unclear (for a detailed discussion, see Hudgins & Allamandola, these proceedings). Another mechanism proposed to explain these variations is a variation in the isotopic ratio, $^{12}\text{C}/^{13}\text{C}$ (Wada et al., 2003).

4. Relative intensity variations

Correlations between the observed intensities of the major UIR features based upon KAO data established the notion of a generic UIR spectrum, which did not vary within the error bars in the (small) sample investigated (e.g. Cohen et al., 1986, 1989). This absence of such variations has sometimes been used as an argument that the carriers cannot be part of an extended PAH family whose detailed composition necessarily must vary when the physical conditions change (Tokunaga & Wada, 1997; Boulanger et al., 1998a). Some variations among the features were however recognized in ground-based data; notably, the weak $3.4\ \mu\text{m}$ feature was shown to vary relative to the main $3.3\ \mu\text{m}$ feature (Geballe et al., 1989; Moorhouse et al., 1989; Joblin et al., 1996a; Sloan et al., 1997) and the $11.2\ \mu\text{m}$ feature was also shown to vary relative to (the wing of) the $7.7\ \mu\text{m}$ feature (Joblin et al., 1996a; Witteborn et al., 1989). As for the peak positions and profiles, the launch of ISO has provided wide spectral coverage with a single instrument of a large and diverse set of objects at high signal-to-noise. This has allowed a detailed re-examination of the issue of variations in the relative intensities of the UIR features and this has led to a reversal of this earlier conclusion. It is now clear that the relative strength of the UIR features varies from source to source and that this provides a tool to determine the characteristics of the emitting population and, eventually, to study the physical conditions in the emitting regions.

4.1. Source to source variations

In their study of the $11\text{--}15\ \mu\text{m}$ UIR features, Hony et al. (2001) discovered that – while all features loosely go together – there are variations in the relative strength of the CC modes in the $6\text{--}9\ \mu\text{m}$ range relative to the CH modes at 3.3 and $11.2\ \mu\text{m}$. Specifically, the $3.3\ \mu\text{m}$ feature correlates quite well with the $11.2\ \mu\text{m}$ feature but they vary by about a factor 5 relative to the $6.2\ \mu\text{m}$ feature (cf., Fig. 4, left panel). Likewise, while the $6.2\ \mu\text{m}$ feature correlates well with the $7.7\ \mu\text{m}$ feature, both features vary relative to the CH features. This can be directly inferred from the spectra shown in Fig. 1. These variations are directly related to object type; that is, while post-AGB objects and PNe are characterized by high $I_{11.2}/I_{6.2}$ and $I_{3.3}/I_{6.2}$ ratios, YSOs, reflection nebulae, and H II regions are displaced to lower values. Thus, the relative intensities of the UIR features reflect the local physical conditions and/or the local history of the emitting population. While a dichotomy between the CH and CC modes exists for the four major UIR features, this does not extend to all CH out-of-plane bending modes. Both the 11.2 and $12.7\ \mu\text{m}$ features corresponds to CH out-of-plane bending modes but their relative strength varies considerably between sources (Fig. 5, left panel).

4.2. Variation with environment

Vermeij et al. (2002) studied H II regions in the Milky Way and the Magellanic Clouds. Consistent with Galactic observations, these authors find correlations between the $I_{7.7}/I_{11.2}$ versus $I_{6.2}/I_{11.2}$ and the $I_{8.6}/I_{11.2}$ versus $I_{6.2}/I_{11.2}$ feature strength ratios (Fig. 4, right panel). These plots suggest an interesting segregation between the sources in the different types of environment (Milky Way –

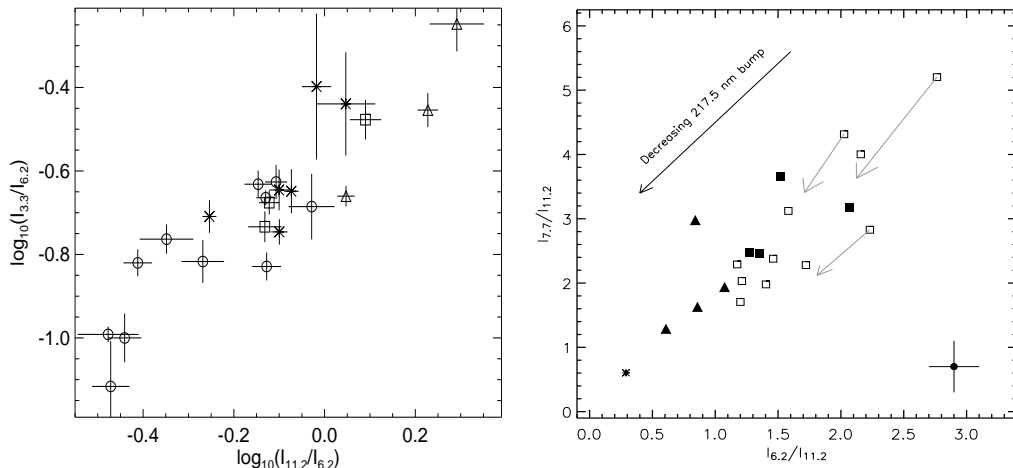


Figure 4. **(left)** The $I_{11.2}/I_{6.2}$ versus the $I_{3.3}/I_{6.2}$ feature strength ratios as derived from the ISO-SWS spectra of various sources. Planetary nebulae are represented by \triangle , H II regions by \circ , reflection nebulae by \square and star forming regions by \star . Courtesy of Hony et al. (2001). **(right)** The $I_{6.2}/I_{11.2}$ versus $I_{7.7}/I_{11.2}$ feature strength ratios as derived from the ISO-SWS and ISO-PHOT spectra of H II regions within the Galaxy and the Magellanic Clouds. The Galactic sources are shown as \square , the non-30 Dor sources as \blacksquare and 30 Dor pointings as \blacktriangle . The asterisk represents the SMC B1#1 molecular cloud (Reach et al., 2000). Courtesy of Vermeij et al. (2002).

LMC – SMC). Furthermore, within the LMC observations, a clear distinction between 30 Doradus and non-30 Doradus pointings is found. In fact, a similar fraction of the total PAH energy is emitted in the 7.7 and 8.6 μm UIR features for the Galactic and Magellanic Cloud sources. In contrast, the fraction of the total PAH flux emitted in the 6.2 μm feature is larger whereas that emitted in the 11.2 μm feature is slightly smaller in the Galactic and non-30 Doradus sources compared to 30 Doradus pointings and the SMC source. We note that the observed variations in the $I_{7.7}/I_{11.2}$ and $I_{6.2}/I_{11.2}$ ratios parallel a variation in the strength of the 2175 Å bump in the UV extinction curve (Vermeij et al., 2002).

4.3. Variations within sources

The intensity studies outlined above have concentrated on the variations between the *entire* integrated UIR spectra from various types of sources, revealing interesting variations with source type and environment. As mentioned earlier, the influence of the local physical conditions (the local radiation field, G_0 ; G_0/n_e which determines the charge balance, ...) are better addressed studying variations within a single source or region of the sky.

It is worth noting that the observed intensity variations in the integrated spectra are necessarily a lower limit to the variations when studied at higher angular resolution. In the simplest case, this is due to the fact that the integrated

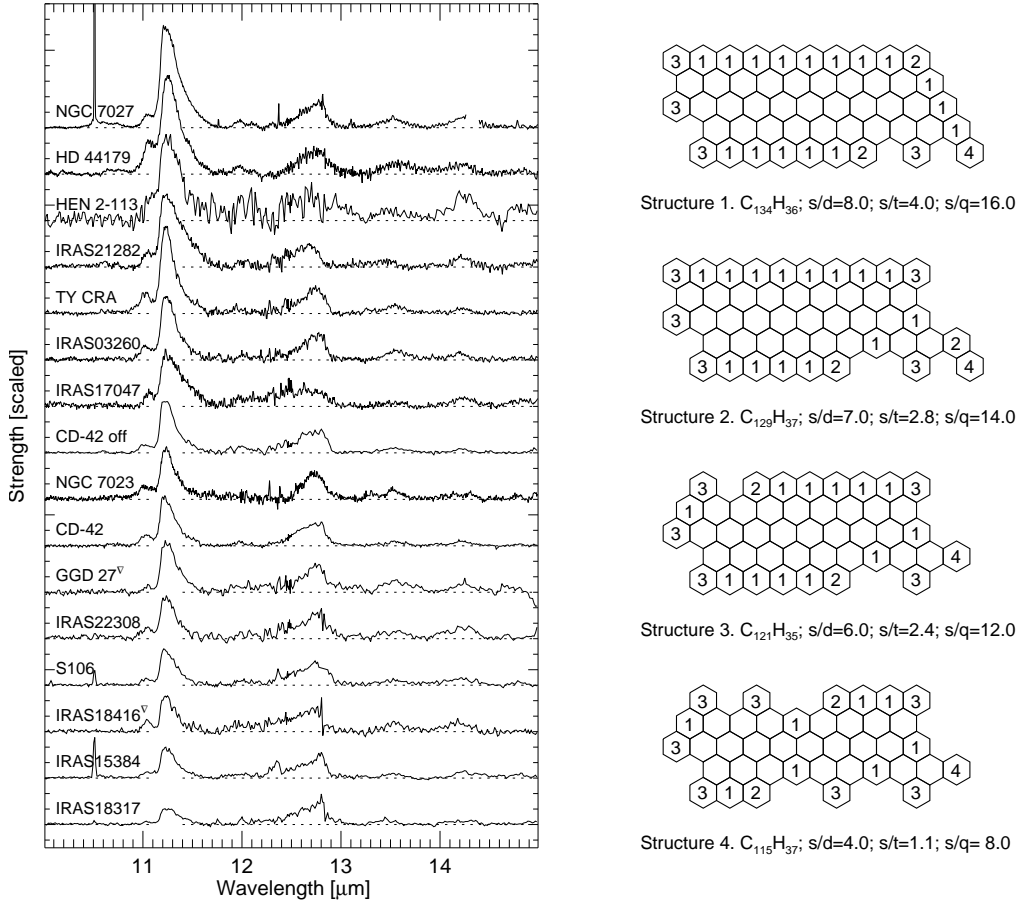


Figure 5. **(left)** An overview of the observed features variations in the out-of-plane bending region. The ISO-SWS spectra are continuum subtracted and scaled to have the same integrated intensity in the $12.7 \mu\text{m}$ UIR feature. **(right)** Examples of molecular structures simultaneously satisfying the structural constraints set by the observed feature strength ratios of the number of solo, duo and trio modes for different interstellar regions. The number of solo, duo, trio and quartet functional groups are noted s , d , t and q respectively. Solo modes are associated with long straight molecular edges while duos and trios correspond to corners. Courtesy of Honny et al. (2001).

spectrum is weighted to the brightest UIR emitting regions and any variations in fainter regions are veiled. In the general case, the different emission features might arise from different locations within the object but still give rise to a “typical” UIR emission spectrum in the integrated spectrum.

As noted above, the existence of variations among the (minor) features within a single source were already established earlier from ground-based observations. The ISOCAM-CVF instrument has allowed to extend the search for such variations to the main CC modes in the $5\text{--}8 \mu\text{m}$ range. This is illustrated

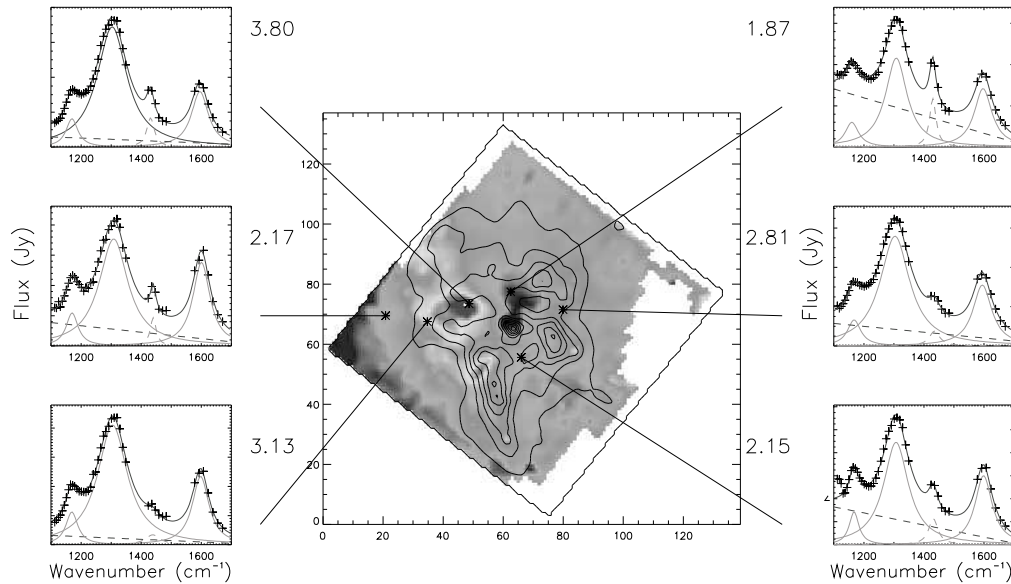


Figure 6. Emission in the $7.7 \mu\text{m}$ UIR feature (contours) and the $I_{7.7}/I_{6.2}$ UIR feature intensity ratio (grey scale) measured in the H 2 region S106 with ISOCAM-CVF. The contours clearly show the central exciting source S106-IR and several large condensations. The spectrum measured at several positions is also displayed. The values on the side give the integrated feature ratio of the 7.7 and $6.2 \mu\text{m}$ UIR features (at 1299 and 1613 cm^{-1} respectively). Courtesy of Joblin et al. (2000).

in Fig. 6 for the bipolar H II region, S106 Joblin et al. (2000). These spectra reveal variations in the relative strength of the 6.2 and $7.7 \mu\text{m}$ features in this source, which these authors link to variations in the molecular composition. In particular, high $I_{7.7}/I_{6.2}$ ratios seem to correspond to clumps of CO emission in the molecular cloud where fresh material is exposed to the strong radiation field (Joblin et al., 2000). These variations seem to be accompanied by a variation in the strength of the UIR features relative to the local continuum. Such a variation in the strength of the CC UIR features relative to the $6 \mu\text{m}$ continuum has also been noted in the H II region M17, on a scale which allowed “mapping” using the $14'' \times 20''$ aperture of the SWS instrument (Verstraete et al., 1996).

4.4. Lack of variations

The previously described studies of UIR feature ratios changing within sources and from source to source, generally refer to regions of high radiation density. Most studies of regions of *low* radiation density, however, conclude that there is a striking lack of variations in the relative intensities of the UIR features in these environments of low illumination. Most notable are the studies performed with the *Infrared Telescope in Space* (IRTS) and ISO of the diffuse ISM (Onaka, 2000; Chan et al., 2001, Onaka, these proceedings) and within reflection nebulae (Uchida et al., 2000). On the average, the relative strength of the UIR features in these nebulae is insensitive to the density of incident radiation field (G_0).

However, these UIR feature ratios show a large spread around these average, and this spread may reflect real variation rather than noise. A recent study on three reflection nebulae by Bregman & Temi (2004) reveals variations in the relative strength of the UIR features with G_0/n_e , which determines the charge balance (e.g. Bakes et al., 2001a, Bakes, these proceedings).

4.5. Implications

The observed variations in the relative strength of the various UIR features provide direct clues to the characteristics of their carriers and their reaction to a changing environment. While this analysis is not yet complete, thanks to a large and dedicated laboratory and theoretical effort, important information is starting to emerge. Here we will focus on two variations and their implications within the framework of the PAH model – the variations in the ratio of the CH to the CC modes feature and the variations in the 11-15 μm range.

The ratio of the CH to CC mode intensity and the charge balance of PAHs Laboratory studies and quantum mechanical calculations have shown that the CC modes are intrinsically weak in neutrals but strong in ions, while this is reversed for neutrals (Ellinger, 1992; Hudgins & Allamandola, 1999; Kim et al., 2001; Piess et al., 2001; Oomens et al., 2001, 2003, Hudgins & Allamandola, these proceedings). Hence, the observed variations in the strength of the CH modes relative to the CC modes may thus reflect a variation in the degree of ionization of the PAHs in these different environments (Joblin et al., 1996b; Hony et al., 2001). This is supported by detailed model calculations of the emission spectra of a family of PAHs, taking realistic molecular properties into account (Bakes et al., 2001a,b, and these proceedings). In this respect, the near constant band-strength ratios for a large range of G_0 under low excitation conditions (Sect. 4.4.), seem puzzling. However, Bakes et al. (2001a) found that the ratios of the infrared emission features do not vary much for G_0/n_e (with n_e the electron density), which determines the PAH charge and which is also difficult to determine observationally. In addition, a seemingly constant ratio over a large range of G_0 would imply a concerted change in electron density (n_e). Such coupled variations in G_0 and n_e are found in reflection nebulae (Young Owl et al., 2002).

The 11-15 μm CH modes and the molecular structure of PAHs Extensive laboratory studies have shown that the peak wavelength of the CH out-of-plane bending mode depends sensitively on the number of adjacent peripheral C-atoms bonded to a H-atom (Bellamy, 1958; Hudgins & Allamandola, 1999, these proceedings). While the details depend slightly on the charge state of the carrier, the 11.2 μm feature can be safely ascribed to lone CH groups (e.g. no H-atoms attached to adjacent C-atoms) and the 12.7 μm feature belongs to a trio's (three adjacent C-atoms each with a H attached). Now, the lone CH groups are part of long straight edges, while trio's are a characteristic of corners in the molecular structure. Variations in the relative strength of the 11.2 to the 12.7 μm feature are thus indicative of variations in the molecular structure of the emitting PAHs. Taking the intrinsic relative strength of these modes into account, possible PAH structures, corresponding to the observed interstellar $I_{11.2}/I_{12.7}$ feature ratios, are illustrated in Fig. 5 (right panel). These variations show that circumstellar

PAHs associated with PNe are characterized by very compact molecular structures. On the other hand, interstellar PAHs have more corners either because they are (on average) much smaller or more irregular larger moieties.

5. UIR features as a diagnostic tool

Since the UIR features originate from such a wide variety of different types of sources and the feature carriers encounter many different astronomical environments, they serve as important probes of these very different emission zones. For example, the presence and strength of the UIR features are generally thought to trace star formation on a Galactic scale. Since the UIR features in extragalactic environments are very similar to those in the Galaxy, they also serve as templates to interpret extragalactic observations.

Concerning galaxies, they are used as qualitative and quantitative diagnostics of the physical processes powering Galactic nuclei (e.g. Genzel et al., 1998; Lutz et al., 1998; Mirabel et al., 1998; Charmandaris et al., 1999; Rigopoulou et al., 1999; Clavel et al., 2000; Helou et al., 2000; Laurent et al., 2000; Tran et al., 2001; Peeters et al., 2004b). The UIR line-to-continuum ratio is on average an order of magnitude smaller for AGNs than for starburst galaxies. This, in combination with emission lines and the dust continuum, is used to distinguish between AGNs, starburst galaxies and heavily obscured galaxies. For example, using this reasoning, it is found that Ultraluminous IR Galaxies (ULIRGs) are mainly powered by starbursts. Consequently, the strength of the UIR features can also probe evolutionary effects in other galaxies on a universal scale. Furthermore, by studying the UIR features in low-metallicity environments (e.g. Vermeij et al., 2002; Madden et al., 2003, Galliano et al., in preparation), they may be tracing the early evolutionary state of galaxies as well as probing the elemental evolution in these galaxies. Finally, a recent study on the use of the UIR features as a quantitative tracer of star formation activity found that the UIRs may better be suited as a probe of B stars which dominate the Galactic stellar energy budget than as a probe of massive star formation (Peeters et al., 2004b). Note as well that the UIR features do not trace ongoing star formation in highly obscured galaxies.

Recent studies on the detailed characteristics of the UIR spectra in galaxies also reveal spectral variations similar to those described above for Galactic objects. The UIR spectrum of galaxies originates from star forming regions and Photo-Dissociation regions. Their Galactic counterparts exhibit UIR features with similar peak positions and profiles, suggesting conditions in these external galaxies are comparable. Although only three galaxies have sufficient S/N in their ISO-SWS spectra to be analyzed in detail they show 3.3, 6.2, 7.7 and 8.6 μm UIR features that are much the same as those associated with H II regions. However, the 11.2 μm profile resembles that of some evolved stars, not H II regions (Peeters et al., 2002; van Dienenhoven et al., 2004). On the other hand, the (relative) intensities of the UIR features in Galactic and extragalactic objects show clear variations. Indeed, intensities between various H II regions in the Milky Way and in the Magellanic Clouds vary greatly (see Sect. 4.). In addition, a study of nearby dwarf galaxies shows a similar range of relative in-

tensities from galaxy to galaxy and within individual galaxies (Madden et al., 2003, Galliano et al., in preparation).

It is clear that the UIR features carry much information on the conditions of the emitting region. However, exploitation of this tool requires a systematic study of the spectral characteristics as a function of the physical conditions in the emitting regions. Such studies carry the promise of a rich diagnostic tool that may probe, in particular, star formation throughout the universe.

6. Summary & Prospects

The UIR emission features dominate the mid-infrared spectrum of almost all sources - Galactic and extragalactic. The UIR spectra in these sources are made up of a rich collection of features. Besides the well-known, most intense UIR features at 3.3, 6.2, 7.7, 8.6, 11.2 and 12.7 μm , many discrete weaker features, subcomponents and very broad structures are observed. It is now firmly established that the detailed characteristics (intensity, peak position, profile) of the UIR features vary from source to source and also spatially within extended sources. In particular, the 6.2 and 7.7 μm features are noteworthy in this respect; while the 6.2 μm feature peak position varies between 6.25–6.3 μm in many PNe, it shifts to 6.2 μm in reflection nebulae and H II regions. Similar behavior is found for the 7.7 μm feature which also consists of two major components, one at 7.6 and one at “7.8” μm . In this case their relative strengths vary between objects. In H II regions and reflection nebulae, the 7.6 μm feature dominates while for most PNe, the “7.8” μm feature takes over. Remarkably, in some post-AGB objects however, this feature has shifted to 8.2 μm . Thus the 6.2 μm component is correlated with the 7.6 μm feature and the 6.25–6.3 μm feature with the “7.8” μm component. While the 3.3 and 11.2 μm features also show some variations in peak position and profile, these are much less pronounced and not as tightly correlated with the variations in the 6.2 and 7.7 μm features. In addition, while the 3.3 and 11.2 μm features correlate tightly, the strength of these features does vary by a factor 5 relative to the 6.2 and 7.7 μm features. Nonetheless, the relative strengths of the features on the 11–15 μm range do vary. These source to source variations in intensity, peak position and profile are also observed spatially within sources and hence are not unique to certain object types. Thus, these variations trace local conditions and reflect the state of the emitting population. Consequently, these variations are emerging as an integral and important part of the UIR studies. They imply that the emission is carried by a family of related chemical compounds whose detailed physical and/or chemical characteristics vary from source to source and within a given source in reaction to the local physical conditions.

Due to their omnipresence, the UIR features are now commonly used as tools for probing objects throughout the universe. They are used as a global diagnostic to reveal the different nature of galaxies, i.e. AGN-dominated, starburst-dominated or heavily obscured. In addition, they are a tracer for star formation and the evolutionary effects in galaxies. On top of this, the detailed UIR spectra which have been observed in a handful of galaxies also show the same significant spectral variations seen in Galactic objects. Thus, these UIR features also hold the promise to serve as powerful and detailed probes of extragalactic objects.

While in the past, progress in this area was limited by astronomical observations, ISO has relocated the astronomical boundary. Today, the richness in spectra and particularly the plethora of spectral variations from source to source and within sources prompt more questions than can be answered with the current laboratory and theoretical data. There have been many comparisons between the spectra of candidate carriers and the astronomical spectra over the years. Due to the large effort put in theoretical and laboratory studies, the agreement with the astronomical spectra are now striking. Nevertheless, thanks to the quality of the new astronomical observations, important differences become apparent which shed further light on the interstellar PAH population. Simultaneously, the wealth of variations observed in the UIR features puts very strong constraints on the candidate carriers.

As with ISO, SIRTf will overwhelm the astronomical community with UIR features. Together with current near- and mid-infrared ground-based instruments, it will probe variations in the spectra of the UIR features on small spatial scales allowing us to fully constrain the variations possible among different objects and to determine, in detail, the interplay of physical conditions, environment and UIR feature characteristics. Due to SIRTf's superb sensitivity, the UIR feature characteristics will also be revealed for a large number of galaxies.

The observational, theoretical and experimental tools are now in place and are being further developed to tackle this vast treasure trove of information which will truly probe most of the universe.

Acknowledgments. We gratefully acknowledge Jesse Bregman, Christine Joblin, Peter Sarre, In-Ok Song who shared their data and preprints with us. We also thank MNRAS for permission to reproduce Fig. 3, right panel. This review wouldn't be the same without ISO, an ESA project with instruments funded by ESA Member States (especially the PI countries: France, Germany, the Netherlands and the United Kingdom) and with the participation of ISAS and NASA. EP acknowledges the financial support of the National Research Council.

References

- Aannestad, P. A. & Kenyon, S. J. 1979, *ApJ*, 230, 771
- Allain, T., Leach, S., & Sedlmayr, E. 1996, *A&A*, 305, 616
- Allamandola, L. J., Hudgins, D. M., & Sandford, S. A. 1999, *ApJ*, 511, L115
- Allamandola, L. J., Tielens, A. G. G. M., & Barker, J. R. 1989, *ApJS*, 71, 733
- Bakes, E. L. O. & Tielens, A. G. G. M. 1994, *ApJ*, 427, 822
- Bakes, E. L. O. & Tielens, A. G. G. M. 1998, *ApJ*, 499, 258
- Bakes, E. L. O., Tielens, A. G. G. M., & Bauschlicher, C. W. 2001a, *ApJ*, 556, 501
- Bakes, E. L. O., Tielens, A. G. G. M., Bauschlicher, C. W., Hudgins, D. M., & Allamandola, L. J. 2001b, *ApJ*, 560, 261
- Barker, J. R., Allamandola, L. J., & Tielens, A. G. G. M. 1987, *ApJ*, 315, L61
- Bauschlicher, J. C. W., Hudgins, D.M., & Allamandola, L.J. 2004, *ApJ*, submitted

- Bellamy, L. 1958, *The infra-red spectra of complex molecules*, 2nd ed. (New York: John Wiley & Sons, Inc.)
- Borghesi, A., Bussoletti, E., & Colangeli, L. 1987, *ApJ*, 314, 422
- Boulanger, F. 1999, in *Solid Interstellar Matter : The ISO Revolution*, (eds.) d'Hendecourt L., Joblin C., Jones A., EDP Sciences, 20
- Boulanger, F., Abergel, A., Bernard, J. P., et al. 1998a, in *ASP Conf. Ser. 132: Star Formation with the Infrared Space Observatory*, (eds.) Yun J. & Liseau R., 15
- Boulanger, F., Abergel, A., Cesarsky, D., et al. 2000, *ISO Beyond Point Sources: Studies of Extended Infrared Emission*, (eds.) Laureijs R. J., Leech K. & Kessler M. F., 455, 91
- Boulanger, F., Boissel, P., Cesarsky, D., & Ryter, C. 1998b, *A&A*, 339, 194
- Bregman, J. 1989, in *IAU Symp. 135: Interstellar Dust*, (eds.) Allamandola L. J. & Tielens A. G. G. M., 109
- Bregman, J. & Temi, P. 2003, in *Astrophysics of Dust*, (ed.) Witt A. N.
- Bregman, J. & Temi, P. 2004, *A&A*, submitted
- Bregman, J. D., Allamandola, L. J., Witteborn, F. C., Tielens, A. G. G. M., & Geballe, T. R. 1989, *ApJ*, 344, 791
- Chan, K., Roellig, T. L., Onaka, T., et al. 2001, *ApJ*, 546, 273
- Charmandaris, V., Laurent, O., Mirabel, I. F., et al. 1999, *Ap&SS*, 266, 99
- Cherchneff, I., Le Teuff, Y. H., Williams, P. M., & Tielens, A. G. G. M. 2000, *A&A*, 357, 572
- Chiar, J. E., Peeters, E., & Tielens, A. G. G. M. 2002, *ApJ*, 579, L91
- Clavel, J., Schulz, B., Altieri, B., et al. 2000, *A&A*, 357, 839
- Cohen, M., Allamandola, L., Tielens, A. G. G. M., et al. 1986, *ApJ*, 302, 737
- Cohen, M., Tielens, A. G. G. M., Bregman, J., et al. 1989, *ApJ*, 341, 246
- Cox, P. & Kessler, M., eds. 1999, *The Universe as Seen by ISO, ESA-SP 427*
- Cr  t  , E., Giard, M., Joblin, C., et al. 1999, *A&A*, 352, 277
- Draine, B. T. 1984, *ApJ*, 277, L71
- Draine, B. T. 2003, in *Carnegie Observatories Astrophysics Series, Vol. 4 : Origin and Evolution of the Elements*, (eds.) A. McWilliam and M. Rauch, in press
- Duley, W. W. & Williams, D. A. 1981, *MNRAS*, 196, 269
- Duley, W. W. & Williams, D. A. 1983, *MNRAS*, 205, 67P
- Dwek, E. 1986, *ApJ*, 302, 363
- Ellinger, Y. 1992, in *IAU Symp. 150: Astrochemistry of Cosmic Phenomena*, (ed.) Singh P. D., 31
- Frenklach, M. & Feigelson, E. D. 1989, *ApJ*, 341, 372
- Geballe, T. R., Lacy, J. H., Persson, S. E., McGregor, P. J., & Soifer, B. T. 1985, *ApJ*, 292, 500
- Geballe, T. R., Tielens, A. G. G. M., Allamandola, L. J., Moorhouse, A., & Brand, P. W. J. L. 1989, *ApJ*, 341, 278
- Genzel, R., Lutz, D., Sturm, E., et al. 1998, *ApJ*, 498, 579

- Gillett, F. C., Forrest, W. J., & Merrill, K. M. 1973, *ApJ*, 183, 87
- Harrington, J. P., Lane, N. J., Borkowski, K. J., Bregman, J. D., & Tsvetanov, Z. I. 1998, *ApJ*, 501, L123
- Helou, G., Lu, N. Y., Werner, M. W., Malhotra, S., & Silbermann, N. 2000, *ApJ*, 532, L21
- Holmlid, L. 2000, *A&A*, 358, 276
- Hony, S., Van Kerckhoven, C., Peeters, E., et al. 2001, *A&A*, 370, 1030
- Hudgins, D. M. & Allamandola, L. J. 1999, *ApJ*, 516, L41
- Joblin, C., Abergel, A., Bregman, J., et al. 2000, ISO beyond the peaks: The 2nd ISO workshop on analytical spectroscopy. (eds.) Salama A., Kessler M. F., Leech K. & Schulz B. ESA-SP456, 49
- Joblin, C., Boissel, P., Leger, A., D'Hendecourt, L., & Defourneau, D. 1995, *A&A*, 299, 835
- Joblin, C., Tielens, A. G. G. M., Allamandola, L. J., & Geballe, T. R. 1996a, *ApJ*, 458, 610
- Joblin, C., Tielens, A. G. G. M., Geballe, T. R., & Wooden, D. H. 1996b, *ApJ*, 460, L119
- Jones, A. P. & d'Hendecourt, L. 2000, *A&A*, 355, 1191
- Kahanpää, J., Mattila, K., Lehtinen, K., Leinert, C., & Lemke, D. 2003, *A&A*, 405, 999
- Kerr, T. H., Hurst, M. E., Miles, J. R., & Sarre, P. J. 1999, *MNRAS*, 303, 446
- Kim, H. S., Wagner, D. R., & Saykally, R. J. 2001, *Phys.Rev.Lett*, 86, 5691
- Laurent, O., Mirabel, I. F., Charmandaris, V., et al. 2000, *A&A*, 359, 887
- Le Page, V., Snow, T. P., & Bierbaum, V. M. 2003, *ApJ*, 584, 316
- Lepp, S. & Dalgarno, A. 1988, *ApJ*, 324, 553
- Lutz, D., Spoon, H. W. W., Rigopoulou, D., Moorwood, A. F. M., & Genzel, R. 1998, *ApJ*, 505, L103
- Madden, S., Galliano, F., & Jones, A. 2003, in *Astrophysics of Dust*, (ed.) Witt A. N.
- Mattila, K., Lemke, D., Haikala, L. K., et al. 1996, *A&A*, 315, L353
- Mirabel, I. F., Vigroux, L., Charmandaris, V., et al. 1998, *A&A*, 333, L1
- Molster, F. J., van den Ancker, M. E., Tielens, A. G. G. M., et al. 1996, *A&A*, 315, L373
- Moorhouse, A., Geballe, T. R., & Allamandola, L. J. 1989, in *Interstellar Dust*, 107
- Moutou, C., Sellgren, K., Léger, A., Verstraete, L., & Le Coupanec, P. 1999a, in *Solid Interstellar Matter : The ISO Revolution*, (eds.) d'Hendecourt L., Joblin C., Jones A., EDP Sciences, 90
- Moutou, C., Sellgren, K., Verstraete, L., & Léger, A. 1999b, *A&A*, 347, 949
- Moutou, C., Verstraete, L., Léger, A., Sellgren, K., & Schmidt, W. 2000, *A&A*, 354, L17

- Moutou, C., Verstraete, L., Sellgren, K., & Léger, A. 1999c, in *The Universe as Seen by ISO*, (eds.) Cox P. & Kessler M. F., ESA SP-427, 727
- Onaka, T. 2000, *Advances in Space Research*, 25, 2167
- Onaka, T., Yamamura, I., Tanabe, T., Roellig, T. L., & Yuen, L. 1996, *PASJ*, 48, L59
- Oomens, J., Sartakov, B. G., Tielens, A. G. G. M., Meijer, G., & von Helden, G. 2001, *ApJ*, 560, L99
- Oomens, J., Tielens, A. G. G. M., Sartakov, B. G., von Helden, G., & Meijer, G. 2003, *ApJ*, 591, 968
- Papoular, R., Conrad, J., Giuliano, M., Kister, J., & Mille, G. 1989, *A&A*, 217, 204
- Pech, C., Joblin, C., & Boissel, P. 2002, *A&A*, 388, 639
- Peeters, E., Allamandola, L. J., Bauschlicher, C. W., et al. 2004a, *ApJ*, submitted
- Peeters, E., Hony, S., Van Kerckhoven, C., et al. 2002, *A&A*, 390, 1089
- Peeters, E., Spoon, H. W. W., & Tielens, A. G. G. M. 2004b, *ApJ*, submitted
- Peeters, E., Tielens, A. G. G. M., Boogert, A. C. A., Hayward, T. L., & Allamandola, L. J. 2004c, *ApJ*, submitted
- Peeters, E., Tielens, A. G. G. M., Roelfsema, P. R., & Cox, P. 1999, *The Universe as Seen by ISO*, (eds.) Cox P. & Kessler M. F., ESA-SP427, 739
- Petrie, S., Stranger, R., & Duley, W. W. 2003, *ApJ*, 594, 869
- Piest, J. A. H., Oomens, J., Bakker, J., von Helden, G., & Meijer, G. 2001, *Spectrochimica Acta*, 57, 717
- Puget, J. L. & Léger, A. 1989, *ARA&A*, 27, 161
- Reach, W. T., Boulanger, F., Contursi, A., & Lequeux, J. 2000, *A&A*, 361, 895
- Rigopoulou, D., Spoon, H. W. W., Genzel, R., et al. 1999, *AJ*, 118, 2625
- Robinson, M. S., Beegle, L. W., & Wdowiak, T. J. 1997, *ApJ*, 474, 474
- Roelfsema, P. R., Cox, P., Tielens, A. G. G. M., et al. 1996, *A&A*, 315, L289
- Sakata, A., Wada, S., Tanabe, T., & Onaka, T. 1984, *ApJ*, 287, L51
- Schutte, W. A., Tielens, A. G. G. M., & Allamandola, L. J. 1993, *ApJ*, 415, 397
- Sellgren, K. 1984, *ApJ*, 277, 623
- Sloan, G. C., Bregman, J. D., Geballe, T. R., Allamandola, L. J., & Woodward, C. E. 1997, *ApJ*, 474, 735
- Snow, T. P. & Witt, A. N. 1995, *Science*, 270, 1455
- Song, I., Kerr, T., McCombie, J., Couch, P., & Sarre, P. 2003a, *MNRAS*, accepted
- Song, I., McCombie, J., Kerr, T., Couch, P., & Sarre, P. 2003b, in *Astrophysics of Dust*, (ed.) Witt A. N.
- Tielens, A. G. G. M. 1990, in *Carbon in the Galaxy: Studies from Earth and Space*, 59
- Tielens, A. G. G. M. 1993, in *Dust and Chemistry in Astronomy*, (eds.) T. J. Millar & D. A. Williams, 103

- Tielens, A. G. G. M. 1997, *Ap&SS*, 251, 1
- Tielens, A. G. G. M. & Allamandola, L. J. 1987, in *ASSL Vol. 134: Interstellar Processes*, 397–469
- Tielens, A. G. G. M. & Charnley, S. B. 1997, *Origins Life Evolution Biosphere*, 27, 23
- Tielens, A. G. G. M., Hony, S., Van Kerckhoven, C., & Peeters, E. 1999, in *The Universe as Seen by ISO*, (eds.) Cox P. & Kessler M. F., *ESA-SP427*, 579
- Tokunaga, A. T., Sellgren, K., Smith, R. G., et al. 1991, *ApJ*, 380, 452
- Tokunaga, A. T. & Wada, S. 1997, *Advances in Space Research*, 19, 1009
- Tran, Q. D., Lutz, D., Genzel, R., et al. 2001, *ApJ*, 552, 527
- Uchida, K. I., Sellgren, K., Werner, M. W., & Houdashelt, M. L. 2000, *ApJ*, 530, 817
- van Diedenhoven, B., Peeters, E., Van Kerckhoven, C., et al. 2004, *ApJ*, submitted
- Van Kerckhoven, C., Hony, S., Peeters, E., et al. 2000, *A&A*, 357, 1013
- Vermeij, R., Peeters, E., Tielens, A. G. G. M., & van der Hulst, J. M. 2002, *A&A*, 382, 1042
- Verstraete, L., Leger, A., D’Hendecourt, L., Defourneau, D., & Dutuit, O. 1990, *A&A*, 237, 436
- Verstraete, L., Pech, C., Moutou, C., et al. 2001, *A&A*, 372, 981
- Verstraete, L., Puget, J. L., Falgarone, E., et al. 1996, *A&A*, 315, L337
- Wada, S., Onaka, T., Yamamura, I., Murata, Y., & Tokunaga, A. T. 2003, *A&A*, 407, 551
- Wagner, D. R., Kim, H., & Saykally, R. J. 2000, *ApJ*, 545, 854
- Witteborn, F. C., Sandford, S. A., Bregman, J. D., et al. 1989, *ApJ*, 341, 270
- Young Owl, R. C., Meixner, M. M., Fong, D., et al. 2002, *ApJ*, 578, 885